CrystEngComm

PAPER

View Article Online
View Journal | View Issue

Cite this: *CrystEngComm*, 2021, **23**, 5241

Trends in rare earth thiophosphate syntheses: $Rb_3Ln(PS_4)_2$ (Ln = La, Ce, Pr), $Rb_{3-x}Na_xLn(PS_4)_2$ (Ln = Ce, Pr; x = 0.50, 0.55), and $RbEuPS_4$ obtained by molten flux crystal growth†

Logan S. Breton, Mark D. Smith and Hans-Conrad zur Loye *

Received 27th May 2021,
Accepted 5th July 2021

DOI: 10.1039/d1ce00703c

rsc.li/crystengcomm

Single crystals of new rubidium rare earth thiophosphates with the formulas $Rb_3Ln(PS_4)_2$ (Ln = La, Ce, Pr), $Rb_{3-x}Na_xLn(PS_4)_2$ (Ln = Ce, Pr; x = 0.50, 0.55), and $RbEuPS_4$ were crystallized out of a molten RbCl flux. The compounds $Rb_3Ln(PS_4)_2$ (Ln = La, Ce, Pr) and $Rb_{3-x}Na_xLn(PS_4)_2$ (Ln = Ce, Pr; x = 0.50, 0.55) both crystallize in the monoclinic crystal system adopting the space groups $P2_1$ and $P2_1/c$, respectively, while $RbEuPS_4$ crystallizes in the orthorhombic crystal system adopting the space group *Pnma*. A survey of all known rubidium rare earth thiophosphates grown using an alkali halide flux revealed trends suggesting that the $Rb_3Ln(PS_4)_2$ and $Rb_{3-x}Na_xLn(PS_4)_2$ families of compounds can be actively targeted over a wide range of temperatures by employing RbCl as at least a component of the flux. Fluorescence measurements were performed on all compounds obtained, revealing resolved f–f transitions in $Rb_3Pr(PS_4)_2$ and $Rb_{2.45(2)}Na_{0.55(2)}Pr(PS_4)_2$ and only single broad emission peaks for $Rb_3Ce(PS_4)_2$ and $Rb_{2.50(6)}Na_{0.50(6)}Ce(PS_4)_2$, behavior characteristic for cerium(III) compounds.

Introduction

Molten flux crystal growth is a popular synthetic method that has become a pillar of modern solid state chemistry due to its continued success in the production of X-ray diffraction quality single crystals of a wide variety of structural families, including metal oxides,[1–3] halides,[4,5] and chalcogenides.[6–11] The use of alkali halide fluxes in particular has resulted in many new single crystalline compounds, while also having the added benefit of the desired crystalline products being easily removed from the product mixture using common solvents, such as water or methanol.

Molten flux synthesis has been shown to be an effective approach for the synthesis of thiophosphate compounds and, over the past decades, has resulted in the successful crystal growth of various thiophosphate compositions incorporating many elements, including transition metals,[12–14] rare earth metals,[15–18] and the actinides.[11,19] The thiophosphates have garnered attention in recent years for their high ionic conductivities[20,21] and for their non-linear optical properties.[22,23] In addition, numerous studies have focused simply on investigating the rich structural chemistry of thiophosphates, which were found to exhibit great diversity and modularity in composition and structure due to the many thiophosphate motifs that exists and that have been incorporated into new crystal structures, such as the thiopyrophosphate building block $P(v)_2S_7^{4-}$,[24,25] the *ortho*-thiophosphate building block $P(v)S_4^{3-}$,[26–32] the hexathiometadiphosphate building block $P(v)_2S_6^{4-}$,[18,33] and the hexathiohypophosphate building block $P(IV)_2S_6^{2-}$.[18,33–37]

Alkali halide fluxes have been demonstrated to be very effective for crystallizing new thiophosphate compounds, such as those prepared in alkali iodide melts by Klepov *et al.*,[34] who reported on numerous rare earth containing thiophosphates, such as the two-dimensional $NaLnP_2S_6$ (Ln = La, Ce, Pr) thiohypophosphates and $CsLnP_2S_7$ (Ln = Pr, Nd, Sm, Gd, Tb, Dy, Ho, Er, Yb, Y) thiopyrophosphates,[34] as well as the family of one-dimensional thiophosphates, $Cs_2NaLn(PS_4)_2$ (Ln = La–Nd, Sm, Gd–Ho).[38] Alkali bromide and chloride fluxes also function well for the synthesis of novel thiophosphates, such as the $ALnP_2S_6$ series[37] grown out of RbBr and CsBr fluxes, and $K_4Nd_2(PS_4)_2(P_2S_6)$ grown out of a KCl flux.[35] Due to the relative sparseness of rubidium containing rare earth thiophosphates, by comparison with those incorporating the other alkali metals, syntheses to create the rubidium analogues of the $Cs_2NaLn(PS_4)_2$ series

Department of Chemistry and Biochemistry, University of South Carolina, Columbia, South Carolina 29208, USA. E-mail: zurLoye@mailbox.sc.edu

† Electronic supplementary information (ESI) available: The ESI contains SEM images, EDS spectra and obtained elemental compositions, as well as a PXRD of the phase pure $RbEuPS_4$ product, and detailed explanations of the X-ray structure solutions for all compounds reported herein. CCDC 2084750–2084755. For ESI and crystallographic data in CIF or other electronic format see DOI: 10.1039/d1ce00703c

created by Klepov *et al.* were carried out by Kutahyali Aslani *et al.*, by employing the same reagents and ratios but replacing the cesium iodide used by Klepov *et al.* with rubidium bromide. The change in flux resulted, however, in a new family of thiophosphates with formulas $Rb_4Ln_2(P_2S_6)(PS_4)_2$ (Ln = La, Ce, Pr, Nd, Sm, Gd).[17]

An overarching goal of solid state chemistry is to achieve the ability to predict structures and to ultimately engineer structures with desired properties. Given the great diversity of thiophosphate structures created in different flux environments, we decided to pursue the synthesis of new thiophosphates by exploring the role of the flux on the formation of thiophosphate products in the hope to better understand the role of the flux as well as to perhaps be able to predict product formation.[6] To probe the effects of the flux on the resulting product formed, experiments were carried out using the same reagents and molar ratios used by Kutahyali Aslani *et al.*, however, this time employing a RbCl flux in place of the previously used RbBr. Herein we report on the synthesis, crystal structures, and select optical measurements of the new rubidium rare earth thiophosphates $Rb_3Ln(PS_4)_2$ (Ln = La, Ce, Pr), $Rb_{3-x}Na_xLn(PS_4)_2$ (Ln = Ce, Pr; x = 0.50, 0.55), and $RbEuPS_4$ obtained by employing the RbCl flux. In addition, we discuss our current thoughts concerning the role of the flux in the creation of rubidium rare earth thiophosphates.

Experimental

Reagents

P_2S_5 (99%, Sigma-Aldrich), Na_2S (Alfa Aesar), *N*,*N*-dimethylformamide (DMF, Sigma-Aldrich, ACS grade), methanol (MeOH, VWR, ACS grade), and La_2S_3 (STREM Chemicals Inc., 99.9%) were all used as received. P_2S_5 and Na_2S were stored and handled in a nitrogen glove bag. Ce_2S_3, Pr_2S_3, and EuS were obtained according to the procedure described in the literature.[39]

Synthesis

The compounds $Rb_3Ln(PS_4)_2$ (Ln = La, Ce, Pr) and $Rb_{3-x}Na_xLn(PS_4)_2$ (Ln = Ce, Pr; x = 0.50, 0.55) were all obtained using the same synthetic conditions. In a nitrogen filled glove bag, powders of Ln_2S_3 (Ln = La, Ce, Pr) (0.265 mmol), Na_2S (1.063 mmol), and P_2S_5 (1.062 mmol) were loaded into a fused silica tube in a 1 : 4 : 4 molar ratio along with 1 gram of RbCl flux. The fused silica tube was flame sealed under vacuum and placed in a box furnace set to ramp up to 820 °C in 1 hour where it dwelled for 20 hours and was subsequently slow cooled to 620 °C in 30 hours. The furnace was then shut off to allow the reaction mixture to cool to room temperature. The compound $RbEuPS_4$ was synthesized using an EuS, Na_2S, P_2S_5 molar ratio of 1 : 2 : 2 which was loaded into a fused silica tube that was evacuated, flame sealed, and placed in a box furnace set to the same temperature profile detailed above. To remove the flux and to isolate the single crystals, all products were sonicated in DMF and then subsequently sonicated in MeOH. The crystalline products were filtered and dried in air. The products are moisture sensitive and were therefore stored in a desiccator. Translucent plate crystals of the $Rb_3Ln(PS_4)_2$ and $Rb_{3-x}Na_xLn(PS_4)_2$ compounds were obtained *via* the same product mixtures for each lanthanide sulfide reagent used. $RbEuPS_4$ was obtained as large yellow/brown plates and was a phase pure product.

Single crystal X-ray diffraction

X-ray intensity data from small irregular crystals were collected at 301(2) K for the compounds $Rb_3Ln(PS_4)_2$ (Ln = Pr, Ce), $Rb_{2.50(6)}Na_{0.50(6)}Ce(PS_4)_2$, and $RbEuPS_4$, at 291(2) K for $Rb_3La(PS_4)_2$, and at 100(2) K for $Rb_{2.45(2)}Na_{0.55(2)}Pr(PS_4)_2$ using a Bruker D8 QUEST diffractometer equipped with a PHOTON-II area detector and an Incoatec microfocus source (Mo Kα radiation, λ = 0.71073 Å). The raw area detector data frames were reduced and corrected for absorption effects using the SAINT+ and SADABS programs.[40,41] Final unit cell parameters were determined by least-squares refinement of large sets of reflections taken from each data set. An initial structural model was obtained with SHELXT.[42] Subsequent difference Fourier calculations and full-matrix least-squares refinement against F^2 were performed with SHELXL-2018 (ref. 43) using the Olex2 interface.[44] Detailed explanations on the X-ray structure determination of all compounds reported herein can be found in the Supporting Information. The crystallographic data and results of the diffraction experiments are summarized in Table 1.

Powder X-ray diffraction

Powder X-ray diffraction (PXRD) data for phase purity confirmation was collected using a polycrystalline sample of $RbEuPS_4$ obtained by grinding single crystals (Fig. S1†). Data was collected on a Bruker D2 PHASER diffractometer using Cu Kα radiation over a 2θ range 10–65° with a step size of 0.02°.

Energy-dispersive spectroscopy (EDS)

EDS was performed on single crystal products using a Tescan Vega-3 SEM equipped with a Thermo EDS attachment. The SEM was operated in low-vacuum mode. Crystals were mounted on an SEM stub with carbon tape and analyzed using a 20 kV accelerating voltage and an 80 s accumulation time. SEM images of the crystals can be found in Fig. S2.† The obtained EDS spectra for each crystal can be found in Fig. S3–S8.† The results of EDS confirm the presence of elements found by single-crystal X-ray diffraction and are summarized in Table S1.†

Optical properties

Photoluminescence data were collected on HORIBA Scientific Standard Microscope Spectroscopy Systems connected with iHR320 Spectrometer and Synchrony detector operating on Labspec 6 software. Spectra were recorded from 400 to 800

Table 1 The crystallographic information for all compounds reported herein

Chemical formula	$Rb_3La(PS_4)_2$	$Rb_3Pr(PS_4)_2$	$Rb_3Ce(PS_4)_2$	$Rb_{2.45(2)}Na_{0.55(2)}Pr(PS_4)_2$	$Rb_{2.50(6)}Na_{0.50(6)}Ce(PS_4)_2$	$RbEuPS_4$
Formula weight	713.74	715.74	714.95	681.32	683.76	396.64
Crystal system	Monoclinic					Orthorhombic
Space group, Z	$P2_1$	$P2_1$	$P2_1$	$P2_1/c$	$P2_1/c$	$Pnma$
a, Å	9.9053(9)	9.8265(3)	9.8512(6)	9.0570(3)	9.1218(4)	17.3308(4)
b, Å	6.7376(6)	6.7613(2)	6.7530(4)	17.3059(6)	17.4862(8)	6.6787(2)
c, Å	11.4553(10)	11.4228(4)	11.4321(7)	9.4252(3)	9.4704(4)	6.43470(10)
β, deg.	90.005(3)	90.2997(12)	90.241(2)	91.8396(13)	91.7907(17)	90
V, Å^3	764.50(12)	758.92(4)	760.52(8)	1476.54(8)	1509.84(11)	744.80(3)
ρ_{calcd}, g cm^{-3}	3.101	3.132	3.122	3.065	3.008	3.537
Radiation (λ, Å)	Mo Kα (0.71073 Å)					
μ, mm^{-1}	13.545	14.040	13.800	12.644	12.317	16.132
T, K	291(2)	301(2)	301(2)	100(2)	301(2)	301(2)
Crystal dim., mm^3	0.040 × 0.030 × 0.020	0.040 × 0.030 × 0.020	0.080 × 0.040 × 0.020	0.040 × 0.020 × 0.020	0.070 × 0.020 × 0.010	0.050 × 0.050 × 0.010
2θ range, deg.	2.718–30.028	2.073–29.142	2.067–32.597	2.250–30.001	2.234–28.310	3.377–29.992
Reflections collected	35 700	27 258	51 419	47 150	35 860	12 334
Data/parameters/restraints	4460/132/2	4082/134/1	5434/134/1	4311/143/0	3763/143/0	1170/43/0
R_{int}	0.0387	0.0412	0.0368	0.0462	0.0720	0.0306
Goodness of fit	1.099	1.181	1.157	1.093	1.129	1.171
$R_1(I > 2\sigma(I))$	0.0493	0.0329	0.0262	0.0297	0.0563	0.0247
wR_2 (all data)	0.0983	0.0541	0.0515	0.0503	0.1267	0.0647

nm using 375 nm laser excitation source power 0.5 mW with 10× UV objective.

Results and discussion

Synthesis

To better understand the role of the flux employed in the molten flux crystal growth of rubidium rare earth thiophosphates, the same starting materials and ratios used by Kutahyali Aslani *et al.* to synthesize the $Rb_4Ln_2(P_2S_6)(PS_4)_2$ series[17] were employed with the only change being the use of a RbCl flux instead of the RbBr flux. This approach resulted in a new series of thiophosphates, specifically, single crystals of the rubidium rare earth thiophosphates $Rb_3Ln(PS_4)_2$ (Ln = La, Ce, Pr) and $Rb_{3-x}Na_xLn(PS_4)_2$ (Ln = Ce, Pr; x = 0.50, 0.55), which were found in the same product mixture. It is important to note that the compound $Rb_{2.61(1)}Na_{0.39(1)}La(PS_4)_2$ was also obtained in the same product mixture as $Rb_3La(PS_4)_2$, however, a similar compound has already been reported in the literature.[15]

As mentioned earlier, one goal of solid state chemistry is to achieve predictive abilities as it pertains to the targeted synthesis of compounds with desired properties. While this goal is far from being accomplished, it is important to document observed patterns and create conversations that may help push this goal further to completion. Our group has had significant success in the growth of alkali rare earth thiophosphates using various alkali halide fluxes and, given the large number of compositions synthesized, this now allows us to look for patterns within this data. Kutahyali Aslani *et al.* attempted to make the rubidium analogues of the $Cs_2NaLn(PS_4)_2$ series created by Klepov *et al.*[38] utilizing the same starting materials and molar ratios however changing the flux from the CsI used by Klepov *et al.* to a RbBr flux. With just the change in flux, a new series of compounds, $Rb_4Ln_2(P_2S_6)(PS_4)_2$ (Ln = La, Ce, Pr, Nd, Sm, and Gd), was obtained. This success of crystallizing brand new rubidium rare earth thiophosphates with just a change in flux motivated the work reported herein. Using the same starting materials and reagent ratios employed by Kutahyali Aslani *et al.*, however, changing from a RbBr to a RbCl flux, the new compounds $Rb_3Ln(PS_4)_2$ (Ln = La, Ce, Pr) and $Rb_{3-x}Na_xLn(PS_4)_2$ (Ln = Ce, Pr; x = 0.50, 0.55) were obtained. Table 2 lists the known rubidium rare earth thiophosphates grown using alkali halide fluxes.

The data in the table demonstrates that the use of different fluxes led to the crystallization of different thiophosphate compositions. To discuss the role of the flux requires, however, that we address two interconnected variables: the identity of the flux and the reaction temperature used. It is known that different products can crystallize at different temperatures depending on the kinetic and thermodynamic processes at play.[6] The change in flux from the RbBr used by Kutahyali Aslani *et al.* to the RbCl used herein also necessitated a change in the reaction temperature used. It is common when using molten fluxes as crystallization media that the reaction temperature is set to 100 °C above the melting point of the flux to ensure the full liquification of the flux and maximizing the likelihood of dissolving all reagents within the flux to achieve the supersaturation necessary for crystal growth upon cooling.[1] The melting point of RbBr is ~700 °C which is the reason that Kutahyali Aslani *et al.* synthesized their crystals at a reaction temperature of 800 °C. The crystals reported herein, using the RbCl flux with a melting point of ~720 °C, dictated that a reaction temperature of 820 °C be used. The 20 °C difference in reaction temperature, while small, nonetheless introduces temperature as a variable. It is likely that in the

Table 2 A table listing the starting materials used, reagent ratios, flux identities, and reaction temperatures for all known rubidium rare earth thiophosphates grown using alkali halide fluxes

Compound	Starting material	Reagent ratios	Flux identity	Reaction temperature	Ref.
$Rb_{2.65}Na_{0.35}La(PS_4)_2$	Ln_2S_3:Na_2S:P_2S_5	1 : 2 : 3	RbCl–NaCl	650 for 48 h	15
$Rb_{2.42}Na_{0.58}Nd(PS_4)_2$	Ln_2S_3:Na_2S:P_2S_5	1 : 2 : 3	RbCl–NaCl	650 for 48 h	15
$Rb_{2.50(6)}Na_{0.50(6)}Ce(PS_4)_2$	Ln_2S_3:Na_2S:P_2S_5	1 : 4 : 4	RbCl	820 for 20 h	This work
$Rb_{2.45(2)}Na_{0.55(2)}Pr(PS_4)_2$	Ln_2S_3:Na_2S:P_2S_5	1 : 4 : 4	RbCl	820 for 20 h	This work
$Rb_3Gd(PS_4)_2$	Ln_2S_3:Na_2S:P_2S_5	1 : 2 : 3	RbCl–NaCl	650 for 48 h	15
$Rb_3Ln(PS_4)_2$ Ln = La, Ce, Pr	Ln_2S_3:Na_2S:P_2S_5	1 : 4 : 4	RbCl	820 for 20 h	This work
$Rb_2NaNd(PS_4)_2$	Ln_2S_3:Na_2S:P_2S_5	1 : 2 : 3	RbI–NaI	650 for 20 h	15
$Rb_4Ln_2(P_2S_6)(PS_4)_2$ Ln = La, Ce, Pr, Nd, Sm, Gd	Ln_2S_3:Na_2S:P_2S_5	1 : 4 : 4	RbBr	800 for 12 h	17
$Rb_3Pr_3(PS_4)_4$	Pr:P:S:RbBr	10 : 12 : 42 : 12	RbBr	950 for 14 days	16
$Rb_3Er_3(PS_4)_4$	Er:P:S:RbBr	4 : 4 : 16 : 3	RbBr	950 for 14 days	16
$RbLaP_2S_6$	Ln:RbBr:S:P	4 : 6 : 18 : 6	RbBr	800 for 24 h	37

case of the $Rb_3Ln(PS_4)_2$ and $Rb_{3-x}Na_xLn(PS_4)_2$ families prepared in an RbCl flux, temperature plays only a minor role in determining product formation. This is because other members of the $Rb_3Ln(PS_4)_2$ and $Rb_{3-x}Na_xLn(PS_4)_2$ families, Table 2, were synthesized in a RbCl–NaCl eutectic flux (melting point: 486 °C) at a reaction temperature of 600 °C.[15] The fact that $Rb_3Ln(PS_4)_2$ and $Rb_{3-x}Na_xLn(PS_4)_2$ crystallizes over a wide temperature range suggests that the identity of the flux predominantly impacts the identity of the product formed. Though the use of a RbBr flux at various temperatures resulted in different products formed, it is interesting that the use of a RbCl flux resulted in the same families of compounds. The observation suggests that these families of compounds can be readily targeted using specifically the RbCl flux as at least one component of the flux. Furthermore, it suggests that it is always worthwhile to explore different alkali halide fluxes after a new composition has been found, as the switch in fluxes may easily lead to additional series of compounds.

The single crystal growth of $RbEuPS_4$ was performed using a 1 : 2 : 2 ratio of EuS, P_2S_5, and Na_2S in order to keep the ratio of lanthanide to phosphorus pentasulfide and sodium sulfide the same as in the other syntheses reported herein. The resulting product, which utilized 1 gram of RbCl flux, was phase pure yellow/brown plates of $RbEuPS_4$. It is important to note that in this structure the lanthanide, europium, is in its 2+ oxidation state where all other compounds reported herein have the lanthanides in their 3+ oxidation state. This is most likely the reason that a different compound, structure, and composition, was obtained for

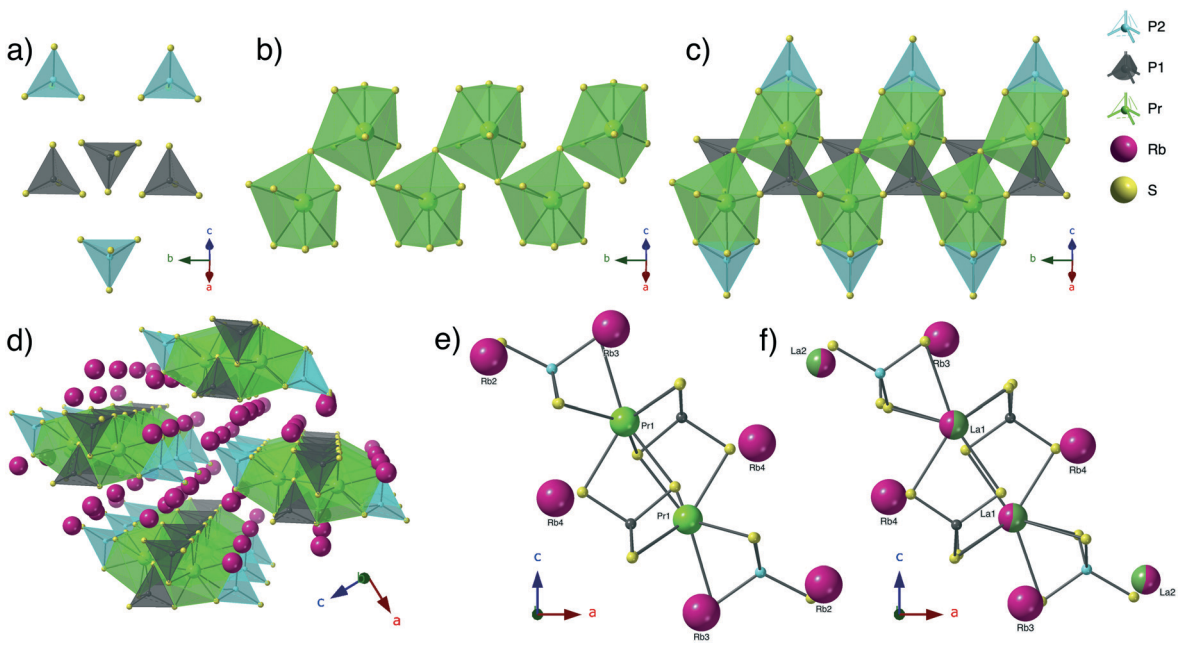

Fig. 1 A schematic of the $Rb_3Ln(PS_4)_2$ (Ln = La, Ce, Pr) structure showing (a) the two PS_4^{3-} units, (b) the connectivity of the LnS_8 polyhedra, (c) the infinite chains of LnS_8 and PS_4^{3-} polyhedra, and (d) the full crystal structure. Fig. 1e and f show a ball and stick representation of the infinite chains of the (e) $Rb_3Pr(PS_4)_2$ and (f) $Rb_3La(PS_4)_2$ structures to visualize where the lanthanum/rubidium site mixing (split pink/green spheres) occurs in Ln = La analogue.

europium, as its ability of taking on the 2+ oxidation state is unique among the rare earths described herein.

Structure description

$Rb_3Pr(PS_4)_2$, and $Rb_3Ce(PS_4)_2$. $Rb_3Pr(PS_4)_2$, and $Rb_3Ce(PS_4)_2$ belong to the $Rb_3Ln(PS_4)_2$ family of thiophosphates and crystallize in a one-dimensional structure type in the monoclinic space group $P2_1$, Fig. 1a–e. The structures consist of two unique PS_4^{3-} tetrahedra and one 8-coordinate LnS_8 highly distorted square antiprism. The LnS_8 polyhedra corner-share with each other creating corrugated infinite chains. Within the chains, the $P(1)S_4^{3-}$ tetrahedra share two edges with adjacent LnS_8 polyhedra and corner share with a third. The $P(2)S_4^{3-}$ thiophosphate tetrahedra then decorate the sides of the LnS_8 polyhedra *via* face-sharing and point into the channels between the infinite chains. These channels are populated with ordered rubidium cations which hold the infinite chains together resulting in the full structure. In these compounds the Ln–S interatomic distances range from 2.8916(19)–3.253(16) Å, the P–S interatomic distances range from 2.0004(18)–2.089(14) Å, and the Rb–S interatomic distances range from 3.290(17)–3.9974(16) Å.

$Rb_3La(PS_4)_2$. $Rb_3La(PS_4)_2$ is isostructural with the other $Rb_3Ln(PS_4)_2$ compounds reported herein however exhibits rubidium/lanthanum site mixing within the structure, Fig. 1f. Of the 4 unique rubidium sites, the Rb1 and Rb2 sites are mixed with lanthanum with La1/Rb1 and La2/Rb2 occupancies of 0.548(4)/0.452(4) and 0.452(4)/0.548(2), respectively, while the Rb3 and Rb4 sites are fully occupied by rubidium. Due to the approximate 50/50 rubidium and lanthanum site mixing, the resulting overall chemical formula is nonetheless the same as those of $Rb_3Pr(PS_4)_2$ and $Rb_3Ce(PS_4)_2$. In this compound the Ln–S interatomic distances, impacted by the site mixing, range from 2.976(8)–3.384(6) Å, the P–S interatomic distances range from 1.984(12)–2.108(11) Å, and the Rb–S interatomic distances range from 3.327(8)–3.949(8) Å.

$Rb_{2.45(2)}Na_{0.55(2)}Pr(PS_4)_2$ and $Rb_{2.50(6)}Na_{0.50(6)}Ce(PS_4)_2$. $Rb_{2.45(2)}Na_{0.55(2)}Pr(PS_4)_2$ and $Rb_{2.50(6)}Na_{0.50(6)}Ce(PS_4)_2$ belong to the $Rb_{3-x}Na_xLn(PS_4)_2$ family of thiophosphates and crystallize in the monoclinic space group $P2_1/c$, Fig. 2. The one-dimensional crystal structure consists of one 9-coordinate LnS_9 polyhedral unit and two unique PS_4^{3-} tetrahedra. The LnS_9 polyhedra alternate between edge- and face-sharing with one another creating infinite LnS_9 chains. Between two face-sharing LnS_9 polyhedra, the $P(1)S_4^{3-}$ tetrahedra face-share with one LnS_9 polyhedra and edge-share with the other. Between two edge-sharing LnS_9 polyhedra, the $P(2)S_4^{3-}$ tetrahedra share one edge with each LnS_9 polyhedra, see Fig. 2d. The resulting $[Ln(PS_4)_2]^{3-}$ infinite chains are held together by 3 unique disordered cationic sites. Sites Rb1 (split into Rb1a and Rb1b) and Rb3 (split into Rb3a and Rb3b) contain solely rubidium cations while site Rb2 is a disordered mixed site of both rubidium and sodium cations. In these compounds, the Ln–S interatomic distances range from 2.8731(10)–3.3038(14) Å, the P–S interatomic distances range from 1.996(4)–2.073(3) Å, and the Rb–S interatomic distances, impacted by the site mixing, range from 3.0046(16)–3.958(13) Å.

$RbEuPS_4$. $RbEuPS_4$ is the rubidium analogue of $KEuPS_4$ (ref. 36) and crystallizes in the orthorhombic space group *Pnma*, Fig. 3. The crystal structure consists of one PS_4^{3-} tetrahedral unit and one 8 coordinate EuS_8 bicapped trigonal prism. The EuS_8 polyhedra edge-share with each other creating a layer of europium polyhedra parallel to the *b*–*c* plane. The edge-sharing of the polyhedra leave trigonal prismatic holes in the layers that are filled by the thiophosphate tetrahedra. The successive layers are connected through rubidium cations which are disordered on their respective sites. In this compound the Eu–S interatomic distances range from 2.9679(16)–3.4516(4) Å, the P–S interatomic distances range from 2.021(2)–2.046(2) Å,

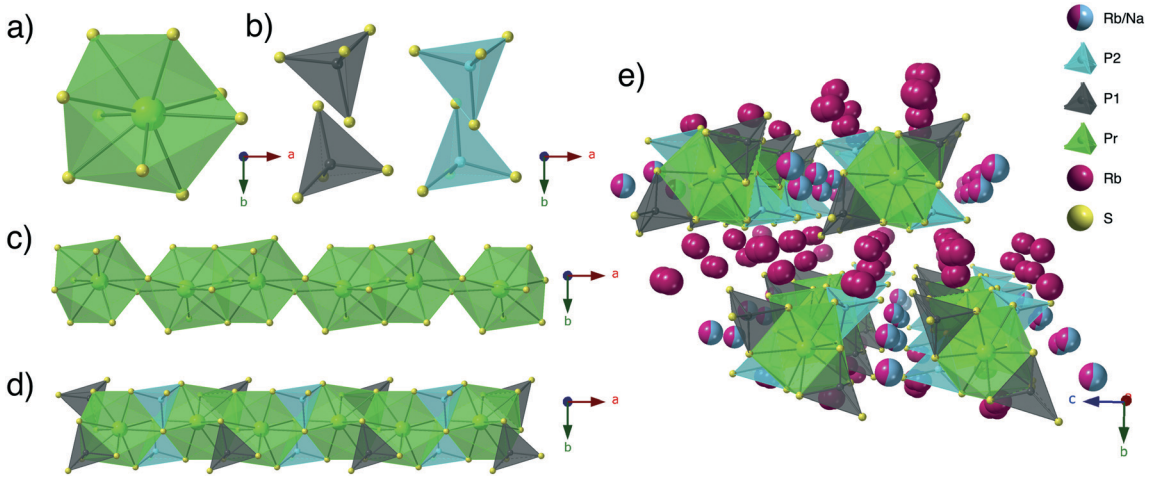

Fig. 2 A schematic of the $Rb_{3-x}Na_xLn(PS_4)_2$ (Ln = Ce, Pr; x = 0.50, 0.55) structure showing (a) the LnS_9 polyhedral unit, (b) the two PS_4^{3-} units, (c) the connectivity of the rare earth polyhedra, (d) the $[Ln(PS_4)_2]^{3-}$ infinite chains, and (e) the full crystal structure.

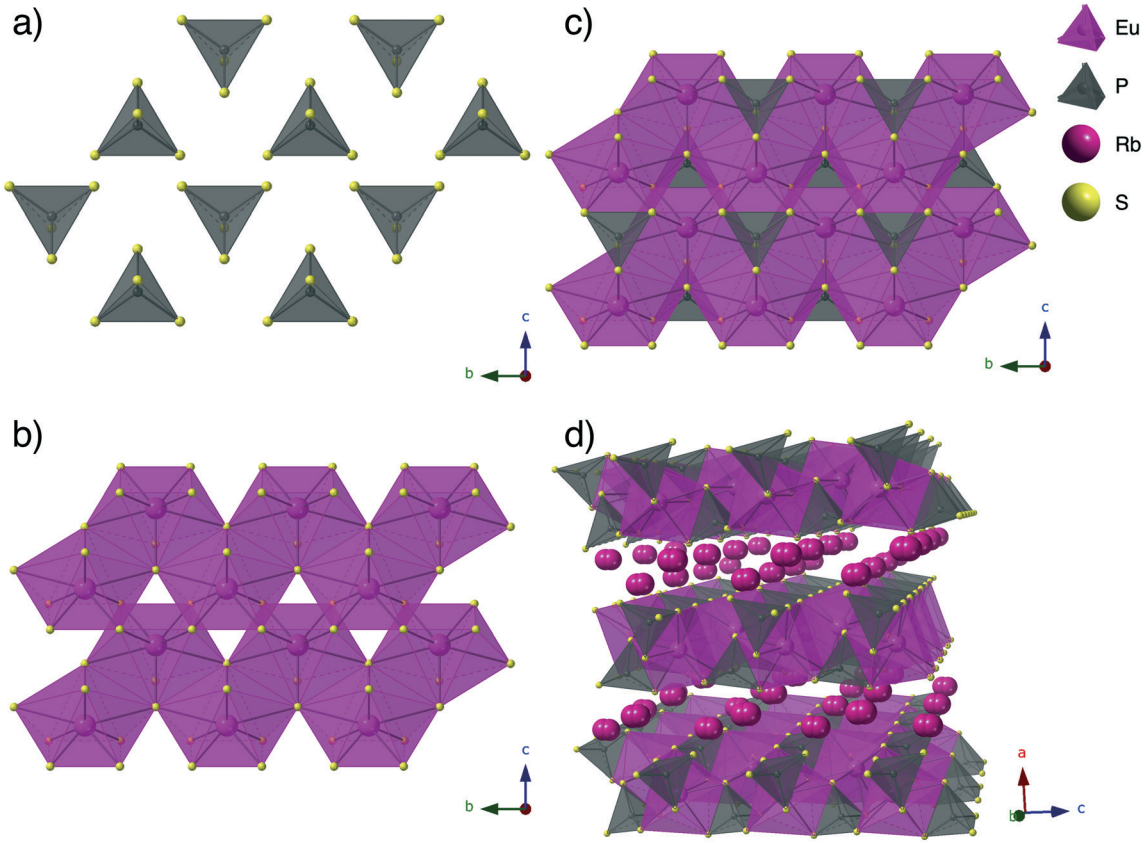

Fig. 3 A schematic of the $RbEuPS_4$ structure showing (a) the PS_4^{3-} unit, (b) the connectivity of the EuS_8 polyhedra, (c) the layers of EuS_8 and PS_4^{3-} polyhedra, and (d) the full crystal structure.

and the Rb–S interatomic distances range from 3.327(8)–3.809(9) Å.

Optical properties

Fluorescence spectra were obtained at an excitation wavelength of 375 nm on single crystals of $Rb_3La(PS_4)_2$, $Rb_3Pr(PS_4)_2$, $Rb_3Ce(PS_4)_2$, $Rb_{2.45(2)}Na_{0.55(2)}Pr(PS_4)_2$, $Rb_{2.50(6)}Na_{0.50(6)}Ce(PS_4)_2$ and $RbEuPS_4$. As expected, there was no fluorescence observed for $Rb_3La(PS_4)_2$, as lanthanum compounds have a $4f^0$ electron configuration.[45] In the case of $RbEuPS_4$, where europium is $4f^7$, one might expect fluorescence; however, no fluorescence was observed from the single crystals of $RbEuPS_4$. The fluorescence spectra for $Rb_3Pr(PS_4)_2$, $Rb_{2.45(2)}Na_{0.55(2)}Pr(PS_4)_2$, $Rb_3Ce(PS_4)_2$, and $Rb_{2.50(6)}Na_{0.50(6)}Ce(PS_4)_2$ are shown in Fig. 4. In the $Rb_3Pr(PS_4)_2$ and $Rb_{2.45(2)}Na_{0.55(2)}Pr(PS_4)_2$ spectra, the expected $^3P_0$

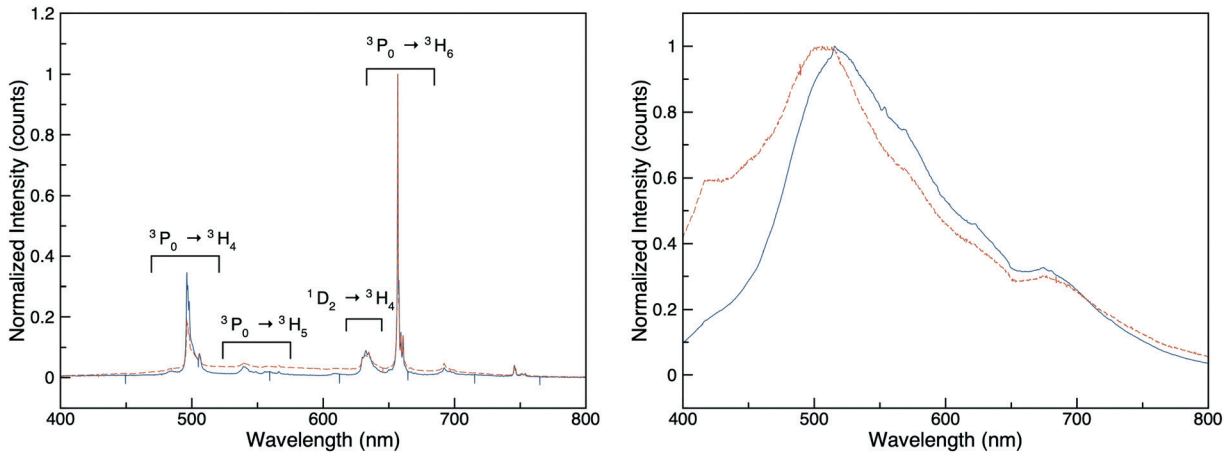

Fig. 4 The emission spectrum of $Rb_3Pr(PS_4)_2$ (blue solid line) and $Rb_{2.45(2)}Na_{0.55(2)}Pr(PS_4)_2$ (orange dashed line) on the left, and that of $Rb_3Ce(PS_4)_2$ (blue solid line) and $Rb_{2.50(6)}Na_{0.50(6)}Ce(PS_4)_2$ (orange dashed line) on the right, taken at an excitation wavelength of 375 nm.

$^3H_4$, $^3P_0 \rightarrow {}^3H_5$, $^1D_2 \rightarrow {}^3H_4$, and $^3P_0 \rightarrow {}^3H_6$ f–f transitions were observed.[46] The fluorescence spectra for the $Rb_3Ce(PS_4)_2$ and $Rb_{2.50(6)}Na_{0.50(6)}Ce(PS_4)_2$, exhibit a single broad peak covering much of the visible range measured, a phenomenon reported for other cerium compounds in the literature.[47–49]

Conclusion

Single crystals of new rubidium rare earth thiophosphates with the formulas $Rb_3Ln(PS_4)_2$ (Ln = La, Ce, Pr), $Rb_{3-x}Na_xLn(PS_4)_2$ (Ln = Ce, Pr; x = 0.50, 0.55), and $RbEuPS_4$ were crystallized out of a molten RbCl flux. The role of the flux in the creation of rubidium rare earth thiophosphates was discussed and contrasted with other thiophosphate families crystallized out of similar halide fluxes. Fluorescence measurements were performed on all compounds obtained, revealing resolved f–f transitions in $Rb_3Pr(PS_4)_2$ and $Rb_{2.45(2)}Na_{0.55(2)}Pr(PS_4)_2$ and only single broad emission peaks for $Rb_3Ce(PS_4)_2$ and $Rb_{2.50(6)}Na_{0.50(6)}Ce(PS_4)_2$, behavior characteristic for cerium(III) compounds.

Author contributions

Breton – conceptualization, investigation, sample synthesis, structure determination, writing. Smith – structure determination, writing, reviewing. zur Loye – conceptualization, methodology, writing, reviewing.

Conflicts of interest

The authors declare no conflicts of interest.

Acknowledgements

Research supported by the US Department of Energy, Office of Basic Energy Sciences, Division of Materials Sciences and Engineering under award DE-SC0018739.

References

1 D. E. Bugaris and H.-C. zur Loye, *Angew. Chem., Int. Ed.*, 2012, **51**, 3780–3811.
2 J. Boltersdorf, N. King and P. A. Maggard, *CrystEngComm*, 2015, **17**, 2225–2241.
3 C. Juillerat, V. V. Klepov, G. Morrison, K. A. Pace and H.-C. zur Loye, *Dalton Trans.*, 2019, **48**, 3162–3181.
4 K. Habermehl, A.-V. Mudring and G. Meyer, *Eur. J. Inorg. Chem.*, 2010, **26**, 4075–4078.
5 V. V. Klepov, C. Juillerat, K. Pace, G. Morrison and H.-C. zur Loye, *Front. Chem.*, 2020, **8**, 518.
6 M. G. Kanatzidis, *Inorg. Chem.*, 2017, **56**, 3158–3173.
7 Y. Wang, J. Wu, Y. Tang, X. Lu, C. Yang, M. Qin, F. Huang, X. Li and X. Zhang, *ACS Appl. Mater. Interfaces*, 2012, **4**, 4246–4250.
8 F. Lissner, S. P. Meyer and T. Schleid, *Z. Naturforsch. B*, 2019, **74**, 99–107.
9 I. Ijjaali, K. Mitchell and J. A. Ibers, *J. Solid State Chem.*, 2004, **177**, 760–764.
10 Y. Yang and J. A. Ibers, *J. Solid State Chem.*, 2000, **149**, 384–390.
11 L. S. Breton, V. V. Klepov and H.-C. zur Loye, *J. Am. Chem. Soc.*, 2020, **142**, 14365–14373.
12 J. Do, K. Lee and H. Yun, *J. Solid State Chem.*, 1996, **125**, 30–36.
13 J.-E. Kwak and J.-S. Yun, *Bull. Korean Chem. Soc.*, 2008, **29**, 273–275.
14 Y. Dong, S. Kim and H. Yun, *Acta Crystallogr., Sect. C: Cryst. Struct. Commun.*, 2005, **61**, i25–i26.
15 M. Usman, M. D. Smith, V. Klepov and H.-C. zur Loye, *Cryst. Growth Des.*, 2019, **19**, 5648–5657.
16 T. Komm and T. Schleid, *J. Solid State Chem.*, 2005, **178**, 454–463.
17 C. Kutahyali Aslani, L. S. Breton, V. Klepov and H.-C. zur Loye, *Dalton Trans.*, 2021, **50**, 1683–1689.
18 L. M. Schoop, R. Eger, J. Nuss, F. Pielnhofer and B. V. Lotsch, *Z. Anorg. Allg. Chem.*, 2017, **643**, 1818–1823.
19 V. V. Klepov and H.-C. zur Loye, *Inorg. Chem.*, 2018, **57**, 11175–11183.
20 M. Tachez, J.-P. Malugani, R. Mercier and G. Robert, *Solid State Ionics*, 1984, **14**, 181–185.
21 R. Schlem, P. Till, M. Weiss, T. Krauskopf, S. P. Culver and W. G. Zeier, *Chem. – Eur. J.*, 2019, **25**, 4143–4148.
22 Z. Li, X. Jiang, M. Zhou, Y. Guo, X. Luo, Y. Wu, Z. Lin and J. Yao, *Inorg. Chem.*, 2018, **57**, 10503–10506.
23 L. Kang, M. Zhou, J. Yao, Z. Lin, Y. Wu and C. Chen, *J. Am. Chem. Soc.*, 2015, **137**, 13049–13059.
24 E.-Y. Goh, E.-J. Kim and S.-J. Kim, *J. Solid State Chem.*, 2001, **160**, 195–204.
25 R. F. Hess, P. L. Gordon, C. D. Tait, K. D. Abney and P. K. Dorhout, *J. Am. Chem. Soc.*, 2002, **124**, 1327–1333.
26 T. Komm and T. Schleid, *Z. Anorg. Allg. Chem.*, 2006, **632**, 42–48.
27 T. Komm and T. Schleid, *J. Alloys Compd.*, 2006, **418**, 106–110.
28 C. Muller, S. Jorgens and A. Mewis, *Z. Anorg. Allg. Chem.*, 2007, **633**, 1633–1638.
29 V. Manriquez, A. Galdamez and D. Guzman-Aguila, *Mater. Res. Bull.*, 2008, **43**, 2469–2475.
30 Y. Klawitter, W. Bensch and C. Wickleder, *Chem. Mater.*, 2006, **18**, 187–197.
31 S. Milot, Y. Wu, C. Nather, W. Bensch and K. O. Klepp, *Z. Anorg. Allg. Chem.*, 2008, **634**, 1575–1580.
32 T. Komm, S. Strobel and T. Schleid, *J. Alloys Compd.*, 2008, **451**, 648–653.
33 A. Kuhn, R. Eger, J. Nuss and B. V. Lotsch, *Z. Anorg. Allg. Chem.*, 2014, **640**, 689–692.
34 V. V. Klepov, L. S. Breton, K. A. Pace, V. Kocevski, T. M. Besman and H.-C. zur Loye, *Inorg. Chem.*, 2019, **58**, 6565–6573.
35 T. Schleid, I. Hartenbach and T. Komm, *Z. Anorg. Allg. Chem.*, 2002, **628**, 7–9.
36 C. R. Evenson and P. K. Dorhout, *Inorg. Chem.*, 2001, **40**, 2884–2891.
37 L. M. Schoop, R. Eger, R. K. Kremer, A. Kuhn, J. Nuss and B. V. Lotsch, *Inorg. Chem.*, 2017, **56**, 1121–1131.

38 V. V. Klepov, M. D. Smith and H.-C. zur Loye, *Inorg. Chem.*, 2020, **59**, 1905–1916.
39 M. Ohta, S. Hirai, H. Kato, V. V. Sokolov and V. V. Bakovets, *Mater. Trans.*, 2009, **50**, 1885–1889.
40 L. Krause, R. Herbst-Irmer, G. M. Sheldrick and D. Stalke, *J. Appl. Crystallogr.*, 2015, **48**, 3–10.
41 *APEX3 Version 2019.1–0 and SAINT+ Version 8.40A*, Bruker Nano, Inc., Madison, WI, United States, 2019.
42 G. M. Sheldrick, *Acta Crystallogr., Sect. A: Found. Adv.*, 2015, **71**, 3–8.
43 G. M. Sheldrick, *Acta Crystallogr., Sect. A: Found. Crystallogr.*, 2008, **64**, 112–122.
44 O. V. Dolomanov, L. J. Bourhis, R. J. Gildea, J. A. K. Howard and H. Puschmann, *J. Appl. Crystallogr.*, 2009, **42**, 339–341.
45 P. S. Peijzel, *J. Solid State Chem.*, 2005, **178**, 448–453.
46 Y.-F. Lin, Y. H. Chang, Y.-S. Chang, B.-S. Tsai and Y.-C. Li, *J. Electrochem. Soc.*, 2006, **153**, G543–G547.
47 E. Banks and R. Ward, *J. Electrochem. Soc.*, 1949, **96**, 297–303.
48 P. N. Hazin, C. Lakshminarayan, L. S. Brinen, J. L. Knee, J. W. Bruno, W. E. Streib and K. Folting, *Inorg. Chem.*, 1988, **27**, 1393–1400.
49 V. V. Klepov, V. Kocevski, T. M. Besmann and H.-C. zur Loye, *CrystEngComm*, 2021, **23**, 831–840.